Published in final edited form as:

Chromosoma. 2019 September ; 128(3): 369–383. doi:10.1007/s00412-019-00713-9.

SIRT7 promotes chromosome synapsis during prophase I of female meiosis

Berta N. Vazquez[1], **Cecilia S. Blengini**[1], **Yurdiana Hernandez**, **Lourdes Serrano**, **Karen Schindler**[*]

Department of Genetics, Rutgers University, 145 Bevier Rd, Piscataway, NJ 08854

Abstract

Sirtuins are NAD^+-dependent protein deacylases and ADP-ribosyltransferases, that are involved in a wide range of cellular processes including genome homeostasis and metabolism. Sirtuins are expressed in human and mouse oocytes yet their role during female gamete development are not fully understood. Here we investigated the role of a mammalian sirtuin member, SIRT7, in oocytes using a mouse knockout (KO) model. *Sirt7* KO females have compromised fecundity characterized by a rapid fertility decline with age, suggesting the existence of a diminished oocyte pool. Accordingly, *Sirt7* KO females produced fewer oocytes and ovulated fewer eggs. Because of the documented role of SIRT7 in DNA repair, we investigated whether SIRT7 regulates prophase I when meiotic recombination occurs. *Sirt7* KO pachynema-like staged oocytes had approximately two-fold increased γH2AX signals associated with regions with unsynapsed chromosomes. Consistent with the presence of asynaptic chromosome regions, *Sirt7* KO oocytes had fewer MLH1 foci (~one less), a mark of crossover-mediated repair, than WT oocytes. Moreover, this reduced level of crossing over is consistent with an observed two-fold increased incidence of aneuploidy in Metaphase II eggs. In addition, we found that acetylated lysine 18 of histone H3 (H3K18ac), an established SIRT7 substrate, was increased at asynaptic chromosome regions suggesting a functional relationship between this epigenetic mark and chromosome synapsis. Taken together, our findings demonstrate a pivotal role for SIRT7 in oocyte meiosis by promoting chromosome synapsis and have unveiled the importance of SIRT7 as novel regulator of the reproductive lifespan.

Keywords

meiosis; synapsis; Sirtuin; SIRT7; oocyte; histone acetylation

Introduction

Transmission of genetic material from one generation to the next requires accurate segregation of chromosomes during meiosis and the formation of high-quality gametes, sperm and egg. During prophase of meiosis I (MI), the integrity of the genome is challenged by induction of hundreds of double strand breaks (DSBs). The first step to repair these

[*]Corresponding author: schindler@dls.rutgers.edu, 848-445-2563.
[1]These authors contributed equally to this work.

breaks requires homologous chromosomes to pair and synapse. In female mammals, defects in this process either trigger the CHK2-dependent DNA damage checkpoint or the meiotic silencing of unsynapsed chromatin (MSUC) pathway (Bolcun-Filas et al. 2014; Cloutier et al. 2015; Rinaldi et al. 2017). The result of triggering these pathways is elimination of defective meiocytes from the pool of oocytes that later go on to be ovulated. Those oocytes that contain fully synapsed chromosomes, repair DSBs using the homolog. Although most repair occurs via non-crossover events, some repair occurs via crossing over. There is a requirement that each homologous pair have at least one recombination event via crossing over, because it ensures homolog linkage that maintains bivalent association critical to protection of gamete euploidy during the completion of MI (Gray and Cohen 2016).

The sirtuin proteins comprise a family of NAD^+ dependent deacetylases critical for maintaining cellular metabolism and genome integrity (Bosch-Presegue and Vaquero 2015). Mammals harbor seven sirtuin genes, denoted *Sirt1* through 7. In mitotic cells, SIRT1, SIRT6 and SIRT7 are primarily located in the nucleus where they perform a myriad of functions related to chromatin organization, transcriptional regulation and DNA damage repair (Vaquero 2009). SIRT2 is both cytoplasmic and nuclear, and it plays important epigenetic roles during cellular division (Serrano et al. 2013; Vaquero et al. 2006). SIRTs 3, 4, and 5 are largely grouped together by their function in mitochondria (van de Ven et al. 2017). Importantly, sirtuins participate in sensing different types of cellular stress, such as genotoxic and oxidative, and in promoting an adequate cellular response to maintain cellular homeostasis (Bosch-Presegue and Vaquero 2014). A key sirtuin function is maintaining genome stability under these forms of stress. Consistent with this role, loss of function of SIRT1, SIRT6 and SIRT7 in mouse models is associated with genome instability resulting either in lethality or reduced lifespan (Cheng et al. 2003; Mostoslavsky et al. 2006; Vazquez et al. 2016). For example, mice lacking *Sirt7* suffer from perinatal lethality and are born at sub-mendelian ratios (Vazquez et al. 2016). Those that do survive to adulthood exhibit multiple signs of accelerated aging including reduced gonadal fat pad content, premature spinal curvature, and a reduced life span. Consistent with a role in maintaining genome stability, fibroblasts derived from these knockout animals have increased levels of DNA double strand breaks (DSBs) that correlate with the presence of replication stress and an impaired DNA damage response. SIRT7 is involved in DNA repair by modulating chromatin structure at DNA damage sites (Vazquez, Thackray et al. 2016). Specifically, SIRT7 is recruited to DNA DSBs where it deacetylates histone H3 at lysine 18 (H3K18). This in turn, facilitates the accumulation of the DNA repair protein 53BP1, thereby favoring the non-homologous end joining repair pathway (NHEJ). Although SIRT7 promotes homologous recombination in a heterologous GFP-based DNA damage reporter system through histone H3K122 desuccinylation (Li et al. 2016), it is not clear that this function occurs *in vivo*. This lack of clarity is because homologous recombination repair is intact in *Sirt7*-deficient fibroblasts (Vazquez et al. 2016). Therefore, its role in homologous recombination is not yet clearly defined.

Although oocyte-specific knockout mouse models to study sirtuin function are lacking, several pieces of evidence have unveiled critical functions of sirtuins in this cell type. For example, SIRT2 and SIRT6 appear important for completion of MI (Han et al. 2015; Zhang et al. 2014). Depletion of either of these sirtuins in prophase I-arrested oocytes

via RNAi, causes meiotic arrest during MI, or in the case of oocytes that complete MI, aneuploid metaphase II (Met II) eggs with spindle defects and increased histone H4 lysine 16 (H4K16) acetylation levels. RNAi-mediated depletion of *Sirt7* in oocytes suggests a role in preventing ROS production possibly by maintaining mitochondrial function, suggesting that it is a protector of oxidative stress (Gao et al. 2018). Despite the known roles of SIRT7 in regulating genome integrity through regulating repair of DSBs in somatic cells, whether it plays a similar role in female gametes is unknown.

Given the critical roles in genome homeostasis, we wanted to examine requirements for SIRT7 in all stages of meiosis in females starting from fetal development through sexual maturity using a KO mouse model. We find a new role for SIRT7 in promoting chromosome synapsis, and absence of SIRT7 correlates with abnormal deacetylation of H3K18 in a pachytene-like stage of prophase I. This defect in chromosome synapsis results in a reduced primordial follicle pool at birth. This reduction causes a premature decline in fertility due to an accelerated exhaustion of gametes in the ovarian reserve. Moreover, oocytes that survive despite persistent asynapsis, are likely the pool that gives rise to aneuploid eggs. Taken together, our findings identify a new role for SIRT7, provide the first example of a sirtuin function during meiotic prophase, and describes an epigenetic modification that is important for regulating chromosome interactions during MI.

Results

Sirt7$^{-/-}$ females have reduced fertility

Because of the known requirement for SIRT7 in regulating genome homeostasis, and the importance of genome integrity during meiosis in the germ line, we wondered if *Sirt7* KO mice had fertility defects. Wild-type (WT) and *Sirt7* KO females were paired with WT males for a time in which it took WT animals to produce 7 litters. The size of the first litter was similar between WT and KOs (Fig. 1a), however, the litter sizes progressively decreased in KOs (Fig. 1b) and no female produced a 7th litter (Fig. 1b). Therefore, *Sirt7* KO females have a premature age-related decline in fertility.

Sirt7$^{-/-}$ females ovulate fewer eggs but oocyte meiotic maturation is normal

To explore the possible causes of the decline in fertility, we first evaluated ovulated Met II-arrested eggs. Compared to WT controls, *Sirt7* KO animals ovulated, on average, two-thirds fewer eggs consistent with the reduction in litter sizes (Fig. 2a). To our surprise, upon evaluation of the eggs, we did not observe abnormalities in chromosome alignment or in spindle morphology (Fig. 2b–c). To more closely evaluate the process of completing MI as a source of producing fewer eggs, we isolated prophase I-arrested oocytes and induced meiotic maturation *in vitro* to Met II. Similar to the reduction in the number of ovulated eggs, we retrieved fewer prophase I-arrested oocytes from KO animals compared to controls (Fig. 2d). Importantly, the process of meiotic maturation appeared normal in KOs because oocytes extruded polar bodies with similar kinetics as WT oocytes (Fig. 2e). Therefore, the reduction in fertility is not caused by defects in completing MI, but could originate from reduced gamete number.

Ovarian reserve of *Sirt7*$^{-/-}$ animals is reduced

To evaluate the source of reduced gamete number, we first analyzed the ovarian reserve of WT and KO animals that were three-weeks of age; an age where they undergo the first wave of folliculogenesis and gamete production (Clarke 2018). Data from histological analyses of hematoxylin/eosin-stained ovarian sections revealed that advanced stages of folliculogenesis were normal: numbers of primary, secondary, pre-antral, and antral follicles were similar between WT and KO animals (Fig. 3a). Importantly, however, KO females had a significantly reduced number of primordial follicles compared to WT controls (10 vs 30 per ovarian section, respectively) (Fig. 3b). This reduction is similar to the reduction in number of ovulated eggs from sexually mature animals, suggesting that the reduced follicle pool is a source of the premature decline in fertility.

Sirt7$^{-/-}$ oocytes have impaired meiotic progression with persistent γH2AX

Because SIRT7 is implicated in the response to DNA damage in somatic cells (Vazquez et al. 2017), the observed reduction of the pool of primordial follicles in KO females could be a consequence of impaired DSB repair. To test this model, we first established parameters to identify the prophase I substages (Pacheco et al. 2018) by staining fetal oocyte chromosome spreads. To this end, we isolated ovaries on embryonic days 16.5 and 18.5 and assessed cytological features of chromosome axes (Fig 4a–c). In WT oocytes, zygonema was defined by the presence of cloud-like patches of γH2AX accompanied with long, thin SYCP3-staining axes. As oocytes entered pachytene (early pachytene), γH2AX began to reduce into foci and SYCP3 axes became shorter and thicker. Pachytene was defined by full homologous chromosome synapsis and the presence of 20 centromeres, marked by ACA staining. The near absence of γH2AX along with separation of SYCP3 axes marked diplotene oocytes, and finally, dictyate-staged oocytes lost continuous SYCP3 signal. Compared to WT, we found a similar distribution of oocytes in zygonema, pachynema, and diplonema stages at embryonic day 16.5 (Fig. 4b). However, at embryonic day 18.5, there was a significant increase in the percentage of KO oocytes in pachynema compared to WT (Fig. 4c), and a trend to have fewer oocytes in diplonema. Therefore, after day 16.5 there is an oocyte developmental delay, arrest or elimination by apoptosis.

Interestingly, we observed KO oocytes that had thick, short pachynema-staged SYCP3 axes, but also presented with small regions of asynapsis that were coincident with clouds of γH2AX (Fig. 4a). To more closely assess pachynema oocytes, we isolated ovaries at embryonic day 17.5. Notably, we observed that although SYCP3 cytologically resembled pachynema stage, 40% of those staged KO oocytes had regions of asynapsis associated with a cloud of γH2AX. We classified these oocytes as pachynema-like (Fig. 4d–e).

Because there was altered prophase I progression coincident with abnormal γH2AX, we wondered if the γH2AX clouds persisted at later developmental stages. To this end, we compared the pattern of γH2AX in late pachynema and diplonema oocytes at embryonic day 18.5. In late pachynema, oocytes from both WT and KO ovaries presented discrete foci of γH2AX, however the amount of γH2AX protein, as measured by average fluorescence intensity, in KO oocytes increased by two-fold (Fig. 4f). Furthermore, KO females had a higher percentage of oocytes in diplonema which were also associated with γH2AX clouds

compared to WT (Fig. 4g). Whether or not this increase marks persistent DNA damage in later prophase I stages, is not known. Taken together, the data suggest that SIRT7 is important for normal prophase I progression.

Sirt7$^{-/-}$ oocytes have reduced levels of crossovers

SIRT7 regulates DNA damage repair in somatic cells (Li et al. 2016; Vazquez et al. 2017). In mammalian meiotic prophase I, H2AX phosphorylation participates in the repair of SPO11-programmed DSBs (Mahadevaiah et al. 2001) and the regulation of chromosome synapsis (Turner et al. 2005). Therefore, we asked if these differences in the pattern of γH2AX reflected defects in DSB repair pathway steps. We first evaluated if Replication Protein A (RPA), a single stranded DNA binding protein, was loaded onto sites of DNA damage and was later resolved upon repair. These steps were assessed by comparing foci in zygonema and pachynema-staged chromosome spreads isolated from ovaries at embryonic day 16.5 (Fig. 5a–c). The data indicated no significant difference in foci number and their resolution between WT and KO oocytes. Next, we assessed the recruitment of the meiosis-specific recombinase, DMC1, which binds to resected DNA and initiates the search for sequence homology at DSBs (Gray and Cohen 2016). Importantly, the number of DMC1 foci that indicated regions of DNA repair were not significantly different between WT and KO animals at zygonema and pachynema (Fig. 5d–f).

Finally, we assessed the last step of meiotic DSB repair by detecting MLH1 foci in late pachytene and pachytene-like-staged oocytes; MLH1 is a cytological marker of crossovers (Anderson et al. 1999). WT oocytes displayed low number of MLH1 foci (20.8± 2.4), possibly reflecting differences between mouse strains (Baier et al. 2014) We find that similar to WT, KO oocytes repaired DSBs via crossing over (Fig. 5g–h). However, we found a statistically significant reduction in MLH1 foci number in KO oocytes (19.2 ± 2.5) indicating that some chromosomes in some oocytes are deficient in cross-over mediated repair (Fig. 5h). Together our findings indicate normal processing of DSBs at earlier stages of the DNA damage response but lower levels of crossovers that are critical for successful chromosome segregation in MI.

Oocytes from *Sirt7*$^{-/-}$ females have chromosome synapsis defects

H2AX phosphorylation occurs at asynaptic homologs (Mahadevaiah et al. 2001) and chromosome synapsis is important for cross over formation. We hypothesized that the observed abnormalities in γH2AX immunostaining in *Sirt7* KO oocytes is due to chromosome synapsis defects because DSB repair appeared intact. We therefore performed an evaluation of the WT pachytene-staged oocytes to those classified as pachytene-like in KO at embryonic day 17.5 (Fig. 4d–e). To confirm that these were sites of asynapsis, we performed immunostaining with an antibody that recognizes HORMAD1, a protein that specifically localizes to asynapsed homologs (Wojtasz et al. 2009). Compared to WT, *Sirt7* KO oocytes had significantly increased numbers of HORMAD1-positive chromosomes (Fig. 6). On average, a KO animal produced 50% of HORMAD1-positive pachytene-like oocytes compared to 20% in WT (Fig. 6b). Significantly, KO oocytes more frequently had 5 or more asynaptic homologs compared to WT oocytes that rarely did (Fig. 6c). These data could help explain a reduction of oocyte numbers at different times in life (fetal, neonatal, and

adult) with the most severe oocytes being eliminated first, and the more minor defective oocytes being eliminated after birth or persisting and giving rise to oocytes that are ovulated. Therefore, the results suggest that SIRT7 promotes chromosome synapsis during prophase I of female meiosis.

Sirt7$^{-/-}$ mice have reduced ovarian reserve at birth and increased numbers of aneuploid eggs

To assess the biological consequences of the synapsis defects, we assessed several parameters. First, because chromosome synapsis defects are associated with oocyte death (Burgoyne et al. 2009), we wondered if the reduced ovarian reserve observed at 3 weeks of age (Fig. 3), could be explained by reduced follicle pool at birth. We assessed histological sections of neonatal ovaries, which contains oocytes still in germ cell cysts or undergoing cyst breakdown to form the primordial follicle pool (Grive and Freiman 2015). We found that whereas WT mice contained ~140 oocytes per ovarian section, this number was reduced by ~30% in KO ovaries (Fig. 7a–b). This reduction does not fully explain the reduction observed at 3 weeks of age, where the primordial pool is reduced by 60% (Fig. 3). We therefore wondered if oocytes were undergoing increased rates of apoptosis in KO ovaries just after birth. Consistent with this hypothesis, we found an increase in the numbers of Caspase 3-positive cells (9 vs 14) in KO ovaries from these neonates (Fig. 7c–d).

Crossover-mediated repair is essential to the formation of chiasma that hold bivalents together until anaphase I onset. Reduced levels of crossing over would therefore predispose oocytes to increased levels of aneuploidy. We determined the levels of achiasmatic chromosomes at metaphase of MI (Met I) by assessing the morphology of bivalents in chromosome spreads. Bivalents held together by one chiasmata have a cruciform shape, whereas homologs that underwent multiple crossovers have bivalents that take on a compact, circular shape. Occasionally we observed WT Met I homologs that were separated, because they did not fit within these morphology parameters. This finding is consistent with occasional reduced numbers of MLH1 foci observed in this strain background (Fig. 5h). Importantly, we did observe, although not statistically significant, an increase in the number of oocytes with at least one separated homolog at Met I (univalents) (Fig. 7e–f). Sister kinetochores of univalent chromosomes can bi-orient and attach to opposite spindle poles at Met I; the result being that sister chromatids separate during MI, giving rise to aneuploid eggs. To determine if KO oocytes are therefore more prone to aneuploidy, we performed *in situ* chromosome spreads of oocytes matured *in vitro* to Met II. Wild-type animals from this strain background produced ~22% aneuploid eggs. We note that this is higher than expected for a WT mouse which is rarely above 5% (Nguyen et al. 2018). It is possible that this strain is more prone to chromosome segregation mistakes when matured *in vitro* or that they are more sensitive to the monastrol treatment used to collapsed the Met II spindle. Most importantly, the incidence of aneuploidy increased in KO eggs to 55% (Fig. 7g–h), similar to the level reported in *Sirt7*-depleted oocytes (Gao et al. 2018). All of the observed aneuploidies observed were prematurely separated sister chromatids (PSSC). Because the presence of univalents in *Sirt7* KO oocytes was minor, other defects, such a mitochondrial dysfunction or premature loss of sister cohesin, could account for the increased aneuploidy incidence.

H3K18 acetylation levels are elevated at regions of asynapsis

Epigenetic modifications play important functions during meiotic progression, (Wang et al. 2017) but a direct role during chromosome synapsis has remained elusive (Crichton et al. 2014). One established SIRT7 substrate is acetylated lysine 18 on histone H3 (H3K18ac) (Barber et al. 2012). We first established stage-specific dynamics of H3K18ac during meiotic prophase in WT oocytes (Fig. 8a–b). We found that H3K18ac is present in zygotene-staged oocytes. This mark is deacetylated in oocytes at pachytene and then re-established upon disassembly of the synaptonemal complex in diplotene. The levels continued to increase in the dictyate stage, consistent with high levels of histone acetylation described in fully grown, prophase I-arrested oocytes (Kageyama et al. 2007).

Because oocytes lacking *Sirt7* have impaired chromosome synapsis (Fig. 6), we compared H3K18ac in pachynema-like oocytes between WT and KO. This acetylation mark was associated with regions of asynapsis in pachynema-like oocytes from WT and KO mice (Fig. 8c). These data suggest that persistent H3K18ac is a consequence of asynapsis.

Discussion

Given the importance of maintaining genome integrity in reproduction and the critical role that SIRT7 has in regulating DNA repair, this particular sirtuin family member as a candidate for regulating meiosis was a high priority to explore. For the first time, we describe that oocytes from *Sirt7* KO animals have defects in chromosome synapsis, which reduces their ovarian reserve thereby causing premature decline in fertility and increased levels of aneuploidy. We note that because this mouse is a whole-body knockout model, we cannot rule out that problems in embryo development, in the uterine environment or other unknown factors could also influence the fecundity of *Sirt7* KO females. However, our results suggest a critical role for SIRT7 in mouse oocytes, supporting previous findings describing oocyte-specific sirtuin functions critical for female gametogenesis and meiosis. Further studies using conditional KO models will be required to decipher the different SIRT7 cell-type-specific functions during meiosis.

To our surprise, oocytes isolated from KO mice and matured *in vitro* to Met II, and eggs derived from hormone-induced ovulation appeared normal. However, upon closer inspection, we observed an increase in the incidence of aneuploidy (~55%) at Met II that either arose as a result of chromosome segregation mistakes during MI or from premature loss of sister chromatid cohesion. In a previous report, depletion of *Sirt7* caused a similar rate of aneuploid egg production. However, the mechanism underlying the source of aneuploidy between this study and the previous could be different. *Sirt7* depletion reportedly caused spindle and chromosomes organization defects because of increased ROS production (Gao et al. 2018). In this KO model, we instead see defects in homolog synapsis and reduced crossing over that likely gives rise to univalent chromosomes at Met I and PSSC at Met II. Whether ROS production is increased in the KO model was not assessed here. Although the authors did not analyze the incidence PSSC in the depletion model, the representative images provided have apparent separation. The assessment of the defects in the whole-body KO allowed studies of early prophase I functions that cannot be addressed in

RNAi-mediated depletion approaches. Together these two studies provide information about the multiple functions of SIRT7 during female meiosis.

In somatic cells, SIRT7-dependent epigenetic regulation is important for the repair of DSBs through the NHEJ (Vazquez et al. 2016) and possibly through homologous recombination (HR) (Li et al. 2016). SIRT7-dependent regulation of NHEJ repair is linked to H3K18 deacetylation and the recruitment of 53BP1. Because HR is the dominant pathway of DSB repair in oocytes (Stringer et al. 2018), we did not yet analyze NHEJ pathway in *Sirt7* KO oocytes. Therefore, whether 53BP1 activity is impaired during meiotic recombination in the absence of SIRT7 will require further investigation. Importantly, our results indicate SIRT7 is a key player during meiotic recombination by ensuring complete synapsis. We find that the most upstream effectors of the DNA damage response, RPA and DMC1, are intact in $Sirt7^{-/-}$ oocytes, which is consistent with previous observations in mitotic cells showing normal H2AX phosphorylation and loading of RAD51 recombinase at damage sites in the absence of SIRT7 (Vazquez et al. 2016). We find instead that SIRT7 activity promotes efficient chromosome synapsis, a process aiming to stabilize chromosome pairing after DSB formation by the loading synaptonemal complex (SC) proteins. A question remains whether the asynaptic regions have persistent DNA damage. Although we evaluated RPA and DMC1 foci in pachynema-like oocytes, this question requires future study. We observed that cross-over formation, a downstream step after homolog synapsis, is reduced on average by one in *Sirt7* KO oocytes. Although we cannot rule out a role for SIRT7 in MLH1 recruitment, this defect is plausibly linked to the impairment of homolog synapsis.

By evaluating the temporal dynamics of a SIRT7 substrate, H3K18ac, we show, for the first time, that global H3K18 acetylation levels fluctuate in a cell cycle-dependent fashion during prophase I. H3K18ac is high in zygonema, declines in pachynema and increases again at diplonema onset. Remarkably, we find that persistent H3K18ac occurs at many asynaptic regions of pachytene-like chromosomes. Pachytene chromosomes are organized into different epigenetic domains (Prakash et al. 2015): chromatin in close proximity to the SC is marked by patches of repressive H3K27me3, while the chromatin organized in loops away from the SC contain active H3K4me3 marks. H3K18ac is observed at regions with impaired chromosome synapsis, it is therefore possible that H3K18 deacetylation is required at chromosome sites where the SC is forming to facilitate chromatin condensation. Alternatively, H3K18ac maybe a consequence of persistent chromosome asynapsis, suggesting a more specific signaling role at unsynapsed axes such as triggering MSUC (Burgoyne et al. 2009). In this sense, H3K18ac may be a new marker of meiotic chromosome asynapsis. Further experiments, including co-localization analysis with HORMADs (Wojtasz et al. 2009) and γH2AX (Mahadevaiah et al. 2001) in pachytene-like meiocytes, should elucidate the validity of this model. In mitotic cells, H3K18 deacetylation is required for efficient binding of several proteins to chromatin (Vazquez et al. 2016) (Tasselli et al. 2016) with important implications in chromatin organization, repression of transcription and responding to DNA damage. SIRT7 has other histones substrates in somatic cells, including succinylated H3K122 (Li et al. 2016) and acetylated H3K36 (Wang et al. 2019). Although SIRT7-catalyzed H3K122 desuccinylation is important for chromatin compaction and DNA repair, the function of SIRT7-dependent H3K36 deacetylation may regulate gene transcription. Further experiments will be required

to define whether these histone modifications are also involved during meiosis to determine the molecular mechanism through which SIRT7 promotes chromosome synapsis and if H3K18 deacetylation is directly involved in this process.

To safeguard genome integrity and prevent the formation of aneuploid eggs, oocytes with meiotic recombination defects are eliminated by different surveillance mechanisms acting in pachynema and diplonema (Cloutier et al. 2015; Roeder and Bailis 2000). Indeed, the results are consistent with the model that KO follicles undergo apoptosis during late embryogenesis and early postnatal development, stages in which these surveillance mechanisms are active. Interestingly, chromosome synapsis defects have more severe consequences on male fertility compared to female fertility (Burgoyne et al. 2009). We note that *Sirt7* KO males are not infertile (data not shown) indicating that spermatocytes are not completely lost in the absence of *Sirt7*. Further investigation will be required to elucidate whether SIRT7 deficiency results in similar or sexually dimorphic phenotypes. We note that ~50% of KO oocytes are normal raising the possibility that an incomplete compensatory mechanism exists. One candidate to explore is SIRT6, which has high structural similarity to SIRT7 (Pan et al. 2011) and also targets H3K18ac for deacetylation in mitotic cells at pericentromeric chromatin (Tasselli et al. 2016). The significant increase in asynaptic chromosomes is the most likely cause driving the early follicle depletion in KO females. Several studies have provided evidence that chromosome asynapsis triggers the activation of either the pachytene DNA damage checkpoint (Rinaldi et al. 2017) or the MSUC pathway (Cloutier et al. 2015). The severity of the asynapsis determines the activation of either of these pathways: severe synaptic defects activates the DNA damage checkpoint whereas moderate or few asynaptic regions induces the MSUC pathway. Because the results indicate that *Sirt7* KO oocytes have few to several chromosomes with asynapsis, it is conceivable that both surveillance mechanisms act to eliminate defective cells. Persistent DNA damage triggers oocyte elimination via the CHK2 pathway (Bolcun-Filas et al. 2014). It would be interesting to analyze oocyte apoptosis in *Sirt7* KO females in the absence of *Chk2*, which, if our model holds true, should partially rescue follicle depletion.

Sirtuins are key players of the aging process and our findings provide new insights about the molecular pathways underlying the anti-aging effects of SIRT7 in reproduction. We show that SIRT7 function is important for the establishment of the pool of primordial follicles early in life and for the overall reproductive lifespan. Because the ovarian reserve of primordial follicles serves as a source for egg development and it is essential for the length of the reproductive lifetime, this work is relevant for the biomedical/reproductive field as it opens novel avenues to understand the causes of premature ovarian dysfunction and infertility in women. It is therefore critical that we understand the contributions that the sirtuins play in generating high quality eggs.

Materials and Methods

Mice and fertility trials

Sirt7$^{-/-}$ deficient mice have been previously described (Vazquez et al. 2016) and were bred in the animal facility at Rutgers University. For fertility assessments, WT and *Sirt7*$^{-/-}$ females were mated with WT males of proven fertility and the total number of pups was

recorded until seven litters were produced by control mice. Animal studies were conducted in accordance with Rutgers University IACUC policies.

Oocyte and egg collection

Prophase I-arrested oocytes were collected as described(Blengini and Schindler 2018) from mice ranging in age from 3–12 weeks mice by mincing the ovaries in MEM/ polyvinylpyrrolidone media containing 2.5 μM milrinone (Sigma-Aldrich; M4659) to prevent oocyte maturation. When oocytes were used for meiosis I analysis, 48h prior collection, females were injected intraperitoneally with 5 I.U. of pregnant mare serum gonadotropin (PMSG). After removing cumulus cells by gentle pipetting, fully grown oocytes with a visible nucleus were matured in CZB media without milrinone in a humified incubator programmed to 5% CO_2 and 37°C. To isolate ovulated metaphase II eggs, females were intraperitoneally injected with 5 units of PMSG followed by 5 I.U. of human chronic gonadotrophin (hCG) 48h later. Females were sacrificed 15h after hormone injection and eggs were collected from oviducts in MEM/ polyvinylpyrrolidone media containing 3 mg/ml hyaluronidase (Sigma-Aldrich, H3506).

Live cell imaging

To measure the dynamics of the polar extrusion of oocytes, prophase I-arrested oocytes were allowed to mature *in vitro* using an EVOS FL Auto Imaging System (Life Technologies) with a 20X objective. The microscope stage was heated to 37°C and 5% CO_2 was maintained using the EVOS Onstage Incubator. Images on bright field of individual cells were acquired every 20 min and processed using NIH Image J software.

Mouse oocyte isolation and chromatin spreads

Sirt7$^{+/-}$ males and females were paired in the afternoon and copulatory plugs were checked the following morning. The day of plugging was considered 0.5 days *post coitum* (d.p.c). Embryos were retrieved from pregnant females and sacrificed at gestational ages 16.5, 17.5, or 18.5 d.p.c and their ovaries were dissected. To release oocytes, ovaries were first swollen in 100μl volume of hypotonic extraction buffer (30mM Tris, pH 8.2, 50mM Sucrose, 17mM Trisodium citrate dihydrate, 5mM EDTA, 0.5mM DTT, 0.1mM PMSF) in a 96-well plate for 40 min at 4°C and then poked using two $27^{1/2}$ G needles in a 50μl drop of 100mM sucrose. Next, the cells that released were transferred into slides coated with 4% paraformaldehyde (PFA) plus 0.15% Triton in PBS, fixed and slowly dried for 2h in a humified chamber. Slides were washed twice in 0.4% Kodak Photo-Flo in 1X PBS and once in 0.4% Kodak Photo-Flo in H_20 for 5 min and finally air-dried. Slides containing chromatin spreads were stored −80°C and, after embryo genotyping results to identify WT and KOs, were processed for immunofluorescence staining.

Metaphase I chromosome spreads was performed as described (Chambon et al. 2013). Oocytes were matured *in vitro* until in metaphase I and were treated with Acidic Tyrode's solution (Millipore Sigma, MR-004-D) to remove the zona pellucida. Then, groups of 7–8 oocytes were transferred to a drop of chromosome spread solution (0.16% Triton-X-100, 3mM DTT, 0.64% paraformaldehyde in distilled water) on glass slides and allowed to slowly air dry prior to processing to detect centromeres and DNA.

Immunofluorescence and image analysis

For fetal chromatin spreads, primary antibodies were diluted into blocking buffer (0.2% BSA, 0.2% Fish Gelatin, 0.1% Tween in PBS) and incubated overnight at 4°C. The following primary antibodies were used: rabbit anti-SYCP3 (1:200, Abcam, ab15093), mouse anti-SYCP3 (1:200, Abcam, ab181746), mouse anti-γH2AX (1:100, Millipore, 05–636), human anti-ACA (1:100, Antibodies incorporated, 15–234), rabbit anti-HORMAD1 (1:1000, Abcam, ab155176), rat anti-RPA (1:150, Cell Signaling, 2208T), mouse anti-DMC1 (1:2000, Abcam ab11054), mouse anti-MLH1 (1:50, BD Pharmingen, 550838) and rabbit anti-H3K18ac (1:1000, Abcam, ab11911). The following morning, slides were washed four times, 15 min each in freshly prepared blocking buffer. A goat anti-mouse Alexa Fluor 488 and goat anti-rabbit-Alexa Fluor 568 secondary antibodies (1:200, Life Technologies, A11029 and A10042, respectively) were diluted in blocking buffer and incubations were carried out for 1h at 37°C in a dark, humified chamber. Samples were washed with blocking buffer as described above and coverslips were mounted on slides with 20μl Vectashield mounting medium containing DAPI.

For fully grown oocytes and ovulated eggs, immunofluorescence staining was performed as described before (Blengini and Schindler 2018). Briefly, cells were fixed in 2% PFA in PBS for 15 min, washed twice in blocking buffer (0.3% BSA containing 0.01% Tween in PBS) and permeabilized in PBS containing 0.2% Triton for 20 min. Oocytes were then blocked for 1h at room temperature and stained with a rabbit anti-α-tubulin-Alexa Fluor 488 (Cell Signaling, 5063S) for 1h at room temperature. After washing, oocytes were mounted in 5μl of Vectashield containing DAPI (Life Technologies, D1306).

Fluorescence images were acquired with either a Zeiss 800, 510 Meta or Leica SP8 confocal microscopes equipped with a 40X, 1.20 NA oil immersion objective. Image analysis was performed using ImageJ (NIH) (Schneider et al. 2012) or Imaris software (Bitplane, A.G.). When foci were quantified, SYCP3-positive axes were used as a mask to limit analysis to specific staining along the SC. When measuring pixel intensity, we used integrated density parameters to take into account the intensity and the area of the signal.

In situ chromosome counting

Chromosome numbers were quantified in metaphase II eggs as described (Stein and Schindler 2011). Briefly, prophase I-arrested oocytes were collected from 6-week-old mice and matured in CZB for 14h. Then eggs were cultured for 2h in 100 μM Monastrol (Sigma, M8515) to disorganize the spindle and disperse the chromosomes. Then eggs were fixed in 2% paraformaldehyde in PBS for 20 minutes and stained with ACA antibody to detect centromeres and DAPI to detect DNA. Images were collected with the Leica SP8 confocal at 0.5 μm z-intervals.

Histological analysis and apoptosis.

Ovaries from newborn and 3-week-old mice were fixed in Modified Davidsons fixative solution (Electron Microscopy Sciences, 64133–50) for 6–12 h and were processed by the Office of Translational Science at Rutgers University for histology services. 5 μm sections of paraffin embedded ovaries were stained with Harris H/E. Ovarian images were acquired

at the 5th, 10th and 15th section in each ovary, under a bright field microscope EVOS FL Auto Imaging System (Life Technologies) with a 20X objective and images were stitched together to project the entire ovary. Ovarian follicles were quantified using morphological criteria(Bristol-Gould et al. 2006). Apoptosis was assessed by immunohistochemistry to detect cleaved caspase 3 (CP3, BioCare Medical # CP229 AA) in section 6 and 11 from ovaries of newborn females (Kimler et al. 2018). Briefly, slides were incubated with CP3-rabbit antibody overnight at 4C followed by detection with a biotinylated goat anti-rabbit IgG secondary antibody (Vectastain Elite ABC HRP kit, Vector LS-J1001) for 1h at room temperature. Endogenous peroxidase blocking was performed by application of 3% H_2O_2/TBS for 15 min at room temperature. Then slides were incubated with Avidin/biotin complex for 30 min at room temperature, and finally the antibody signal was detected with DAB (3,3'-diaminobenzidine) HRP substrate kit (DAB peroxidase substrate kit, VECTOR SK4100). Tissues were counterstained with hematoxylin. Images were acquired under bright field with the EVOS FL Auto Imaging System (Life Technologies) with a 20X objective.

Statistical analysis

Unless otherwise indicated, results are shown as the mean ± standard error (SEM), with *P*-values calculated by Student's t-test.

Acknowledgments

The authors thank Jay Tischfield for project support, Karen Berkowitz for technical advice and helpful discussions, Kim McKim and Alejandro Vaquero for critical reading of the manuscript, and Marianne Polunas for processing ovarian tissues. This study was supported by a grant from the Human Genetics Institute of New Jersey and an NIH grant to KS (R01-GM112801).

References

Anderson LK, Reeves A, Webb LM, Ashley T (1999) Distribution of crossing over on mouse synaptonemal complexes using immunofluorescent localization of MLH1 protein Genetics 151:1569–1579 [PubMed: 10101178]

Baier B, Hunt P, Broman KW, Hassold T (2014) Variation in genome-wide levels of meiotic recombination is established at the onset of prophase in mammalian males PLoS Genet 10:e1004125 doi:10.1371/journal.pgen.1004125 [PubMed: 24497841]

Barber MF et al. (2012) SIRT7 links H3K18 deacetylation to maintenance of oncogenic transformation Nature 487:114–118 doi:10.1038/nature11043 [PubMed: 22722849]

Blengini CS, Schindler K (2018) Immunofluorescence Technique to Detect Subcellular Structures Critical to Oocyte Maturation Methods Mol Biol 1818:67–76 doi:10.1007/978-1-4939-8603-3_8 [PubMed: 29961256]

Bolcun-Filas E, Rinaldi VD, White ME, Schimenti JC (2014) Reversal of female infertility by Chk2 ablation reveals the oocyte DNA damage checkpoint pathway Science 343:533–536 doi:10.1126/science.1247671 [PubMed: 24482479]

Bosch-Presegue L, Vaquero A (2014) Sirtuins in stress response: guardians of the genome Oncogene 33:3764–3775 doi:10.1038/onc.2013.344 [PubMed: 23995787]

Bosch-Presegue L, Vaquero A (2015) Sirtuin-dependent epigenetic regulation in the maintenance of genome integrity FEBS J 282:1745–1767 doi:10.1111/febs.13053 [PubMed: 25223884]

Bristol-Gould SK et al. (2006) Postnatal regulation of germ cells by activin: the establishment of the initial follicle pool Dev Biol 298:132–148 doi:10.1016/j.ydbio.2006.06.025 [PubMed: 16930587]

Burgoyne PS, Mahadevaiah SK, Turner JM (2009) The consequences of asynapsis for mammalian meiosis Nat Rev Genet 10:207–216 doi:10.1038/nrg2505 [PubMed: 19188923]

Chambon JP, Hached K, Wassmann K (2013) Chromosome spreads with centromere staining in mouse oocytes Methods Mol Biol 957:203–212 doi:10.1007/978-1-62703-191-2_14 [PubMed: 23138954]

Cheng HL et al. (2003) Developmental defects and p53 hyperacetylation in Sir2 homolog (SIRT1)-deficient mice Proc Natl Acad Sci U S A 100:10794–10799 doi:10.1073/pnas.1934713100 [PubMed: 12960381]

Clarke HJ (2018) Regulation of germ cell development by intercellular signaling in the mammalian ovarian follicle Wiley Interdiscip Rev Dev Biol 7 doi:10.1002/wdev.294

Cloutier JM, Mahadevaiah SK, ElInati E, Nussenzweig A, Toth A, Turner JM (2015) Histone H2AFX Links Meiotic Chromosome Asynapsis to Prophase I Oocyte Loss in Mammals PLoS Genet 11:e1005462 doi:10.1371/journal.pgen.1005462 [PubMed: 26509888]

Crichton JH, Playfoot CJ, Adams IR (2014) The role of chromatin modifications in progression through mouse meiotic prophase J Genet Genomics 41:97–106 doi:10.1016/j.jgg.2014.01.003 [PubMed: 24656230]

Gao M et al. (2018) SIRT7 functions in redox homeostasis and cytoskeletal organization during oocyte maturation FASEB J:fj201800078RR doi:10.1096/fj.201800078RR

Gray S, Cohen PE (2016) Control of Meiotic Crossovers: From Double-Strand Break Formation to Designation Annu Rev Genet 50:175–210 doi:10.1146/annurev-genet-120215-035111 [PubMed: 27648641]

Grive KJ, Freiman RN (2015) The developmental origins of the mammalian ovarian reserve Development 142:2554–2563 doi:10.1242/dev.125211 [PubMed: 26243868]

Han L et al. (2015) Sirt6 depletion causes spindle defects and chromosome misalignment during meiosis of mouse oocyte Sci Rep 5:15366 doi:10.1038/srep15366 [PubMed: 26481302]

Kageyama S, Liu H, Kaneko N, Ooga M, Nagata M, Aoki F (2007) Alterations in epigenetic modifications during oocyte growth in mice Reproduction 133:85–94 doi:10.1530/REP-06-0025 [PubMed: 17244735]

Kimler BF, Briley SM, Johnson BW, Armstrong AG, Jasti S, Duncan FE (2018) Radiation-induced ovarian follicle loss occurs without overt stromal changes Reproduction 155:553–562 doi:10.1530/REP-18-0089 [PubMed: 29636407]

Li L et al. (2016) SIRT7 is a histone desuccinylase that functionally links to chromatin compaction and genome stability Nat Commun 7:12235 doi:10.1038/ncomms12235 [PubMed: 27436229]

Mahadevaiah SK et al. (2001) Recombinational DNA double-strand breaks in mice precede synapsis Nat Genet 27:271–276 doi:10.1038/85830 [PubMed: 11242108]

Mostoslavsky R et al. (2006) Genomic instability and aging-like phenotype in the absence of mammalian SIRT6 Cell 124:315–329 doi:10.1016/j.cell.2005.11.044 [PubMed: 16439206]

Nguyen AL et al. (2018) Genetic Interactions between the Aurora Kinases Reveal New Requirements for AURKB and AURKC during Oocyte Meiosis Curr Biol 28:3458–3468 e3455 doi:10.1016/j.cub.2018.08.052 [PubMed: 30415701]

Pacheco S et al. (2018) ATR is required to complete meiotic recombination in mice Nat Commun 9:2622 doi:10.1038/s41467-018-04851-z [PubMed: 29977027]

Pan PW, Feldman JL, Devries MK, Dong A, Edwards AM, Denu JM (2011) Structure and biochemical functions of SIRT6 J Biol Chem 286:14575–14587 doi:10.1074/jbc.M111.218990 [PubMed: 21362626]

Prakash K et al. (2015) Superresolution imaging reveals structurally distinct periodic patterns of chromatin along pachytene chromosomes Proc Natl Acad Sci U S A 112:14635–14640 doi:10.1073/pnas.1516928112 [PubMed: 26561583]

Rinaldi VD, Bolcun-Filas E, Kogo H, Kurahashi H, Schimenti JC (2017) The DNA Damage Checkpoint Eliminates Mouse Oocytes with Chromosome Synapsis Failure Mol Cell 67:1026–1036 e1022 doi:10.1016/j.molcel.2017.07.027 [PubMed: 28844861]

Roeder GS, Bailis JM (2000) The pachytene checkpoint Trends Genet 16:395–403 [PubMed: 10973068]

Schneider CA, Rasband WS, Eliceiri KW (2012) NIH Image to ImageJ: 25 years of image analysis Nat Methods 9:671–675 [PubMed: 22930834]

Serrano L et al. (2013) The tumor suppressor SirT2 regulates cell cycle progression and genome stability by modulating the mitotic deposition of H4K20 methylation Genes Dev 27:639–653 doi:10.1101/gad.211342.112 [PubMed: 23468428]

Stein P, Schindler K (2011) Mouse oocyte microinjection, maturation and ploidy assessment J Vis Exp doi:10.3791/2851

Stringer JM, Winship A, Liew SH, Hutt K (2018) The capacity of oocytes for DNA repair Cell Mol Life Sci 75:2777–2792 doi:10.1007/s00018-018-2833-9 [PubMed: 29748894]

Tasselli L et al. (2016) SIRT6 deacetylates H3K18ac at pericentric chromatin to prevent mitotic errors and cellular senescence Nat Struct Mol Biol 23:434–440 doi:10.1038/nsmb.3202 [PubMed: 27043296]

Turner JM, Mahadevaiah SK, Fernandez-Capetillo O, Nussenzweig A, Xu X, Deng CX, Burgoyne PS (2005) Silencing of unsynapsed meiotic chromosomes in the mouse Nat Genet 37:41–47 doi:10.1038/ng1484 [PubMed: 15580272]

van de Ven RAH, Santos D, Haigis MC (2017) Mitochondrial Sirtuins and Molecular Mechanisms of Aging Trends Mol Med 23:320–331 doi:10.1016/j.molmed.2017.02.005 [PubMed: 28285806]

Vaquero A (2009) The conserved role of sirtuins in chromatin regulation Int J Dev Biol 53:303–322 doi:10.1387/ijdb.082675av [PubMed: 19378253]

Vaquero A et al. (2006) SirT2 is a histone deacetylase with preference for histone H4 Lys 16 during mitosis Genes Dev 20:1256–1261 doi:10.1101/gad.1412706 [PubMed: 16648462]

Vazquez BN, Thackray JK, Serrano L (2017) Sirtuins and DNA damage repair: SIRT7 comes to play Nucleus 8:107–115 doi:10.1080/19491034.2016.1264552 [PubMed: 28406750]

Vazquez BN et al. (2016) SIRT7 promotes genome integrity and modulates non-homologous end joining DNA repair EMBO J 35:1488–1503 doi:10.15252/embj.201593499 [PubMed: 27225932]

Wang L, Xu Z, Khawar MB, Liu C, Li W (2017) The histone codes for meiosis Reproduction 154:R65–R79 doi:10.1530/REP-17-0153 [PubMed: 28696245]

Wang WW et al. (2019) A Click Chemistry Approach Reveals the Chromatin-Dependent Histone H3K36 Deacylase Nature of SIRT7 J Am Chem Soc doi:10.1021/jacs.8b12083

Wojtasz L et al. (2009) Mouse HORMAD1 and HORMAD2, two conserved meiotic chromosomal proteins, are depleted from synapsed chromosome axes with the help of TRIP13 AAA-ATPase PLoS Genet 5:e1000702 doi:10.1371/journal.pgen.1000702 [PubMed: 19851446]

Zhang L, Hou X, Ma R, Moley K, Schedl T, Wang Q (2014) Sirt2 functions in spindle organization and chromosome alignment in mouse oocyte meiosis FASEB J 28:1435–1445 doi:10.1096/fj.13-244111 [PubMed: 24334550]

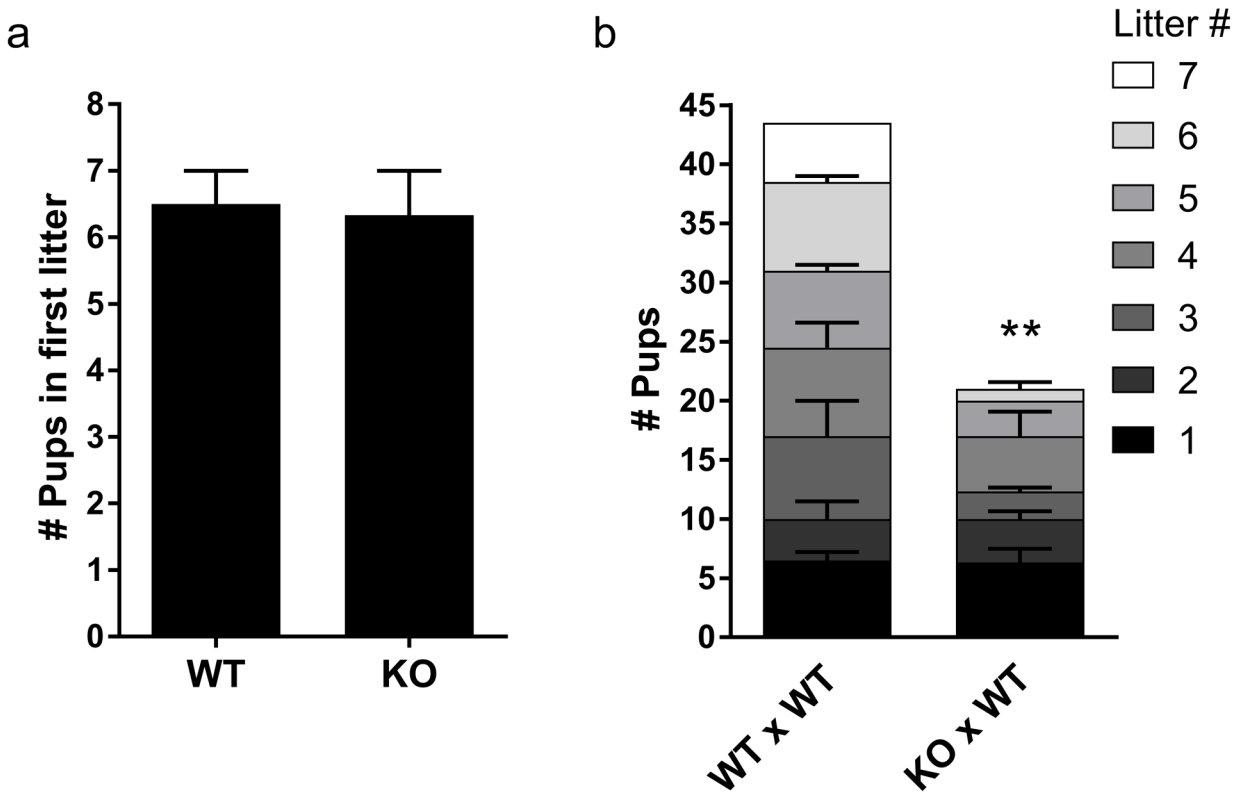

Fig. 1. *Sirt7*$^{-/-}$ females are subfertile and experience age dependent infertility

(a) Number of pups produced by WT and *Sirt7*$^{-/-}$ (KO) females in the first litter after mating. **(b)** Litter and pup numbers from fertility trials. Genotypes are written by female X male. Graphs represent the mean ± SEM of WT (n =2) or KO (n=3) females. ** P< 0.01.

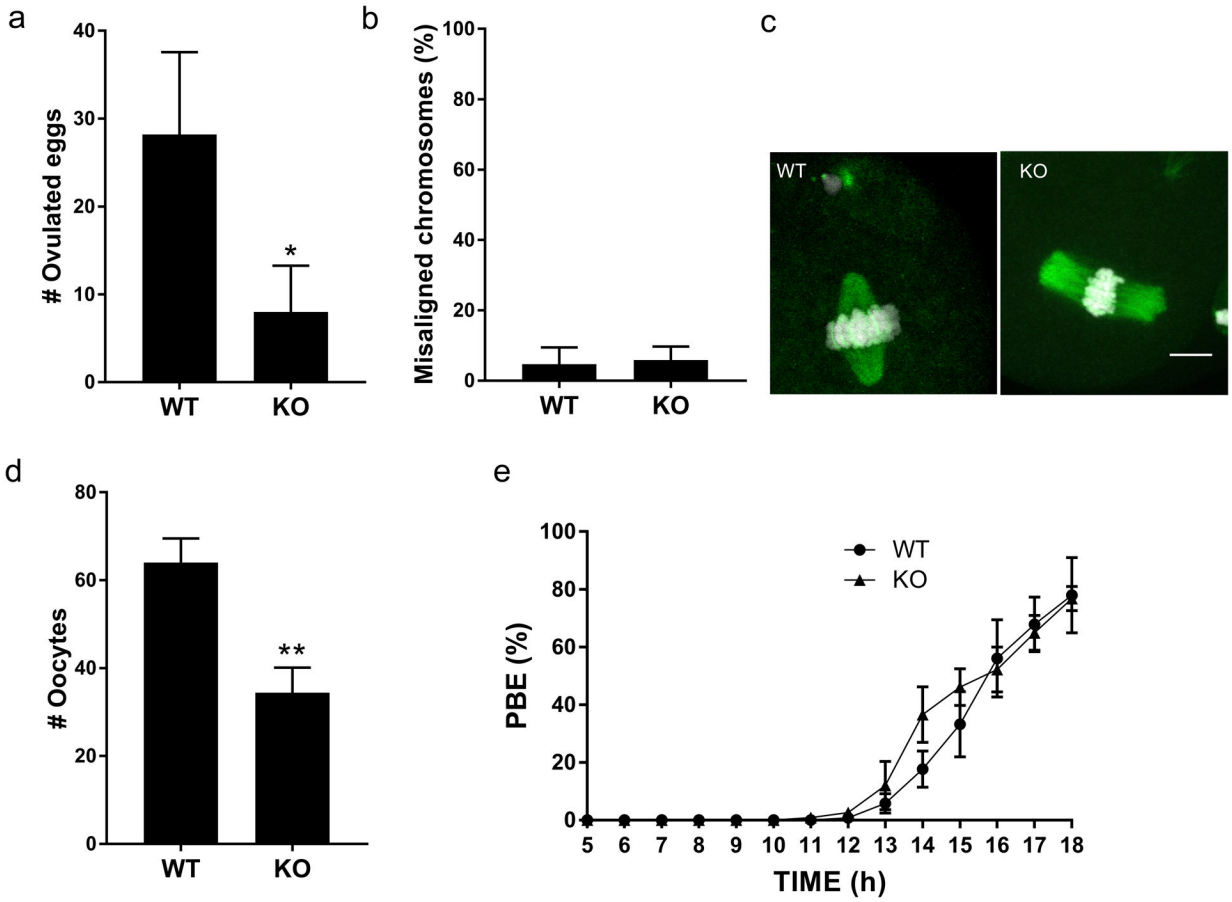

Fig. 2. *Sirt7*$^{-/-}$ females contain fewer gametes

(a) Number of ovulated eggs isolated after hormone stimulation from wild-type (WT) and *Sirt7*$^{-/-}$ (KO) females. Graph represents the mean ±SEM (n=5 mice /genotype). **(b)** Percent of misaligned chromosomes from ovulated eggs. Data represents the mean ±SEM (n=3 animals/per genotype; ~40 eggs were evaluated). **(c)** Representative images of WT and KO eggs stained to detect DNA (DAPI, white) and the spindle (α-tubulin, green). **(d-e)** Prophase I-arrested oocytes from WT and KO animals were collected (d) and *in vitro* matured on a live-cell imager for 18h and the time of polar body extrusion (PBE) (e) was measured. Graph represents mean ±SEM (n=3 animals/genotype). * P< 0.05; ** P < 0.01; scale bar, 10μm

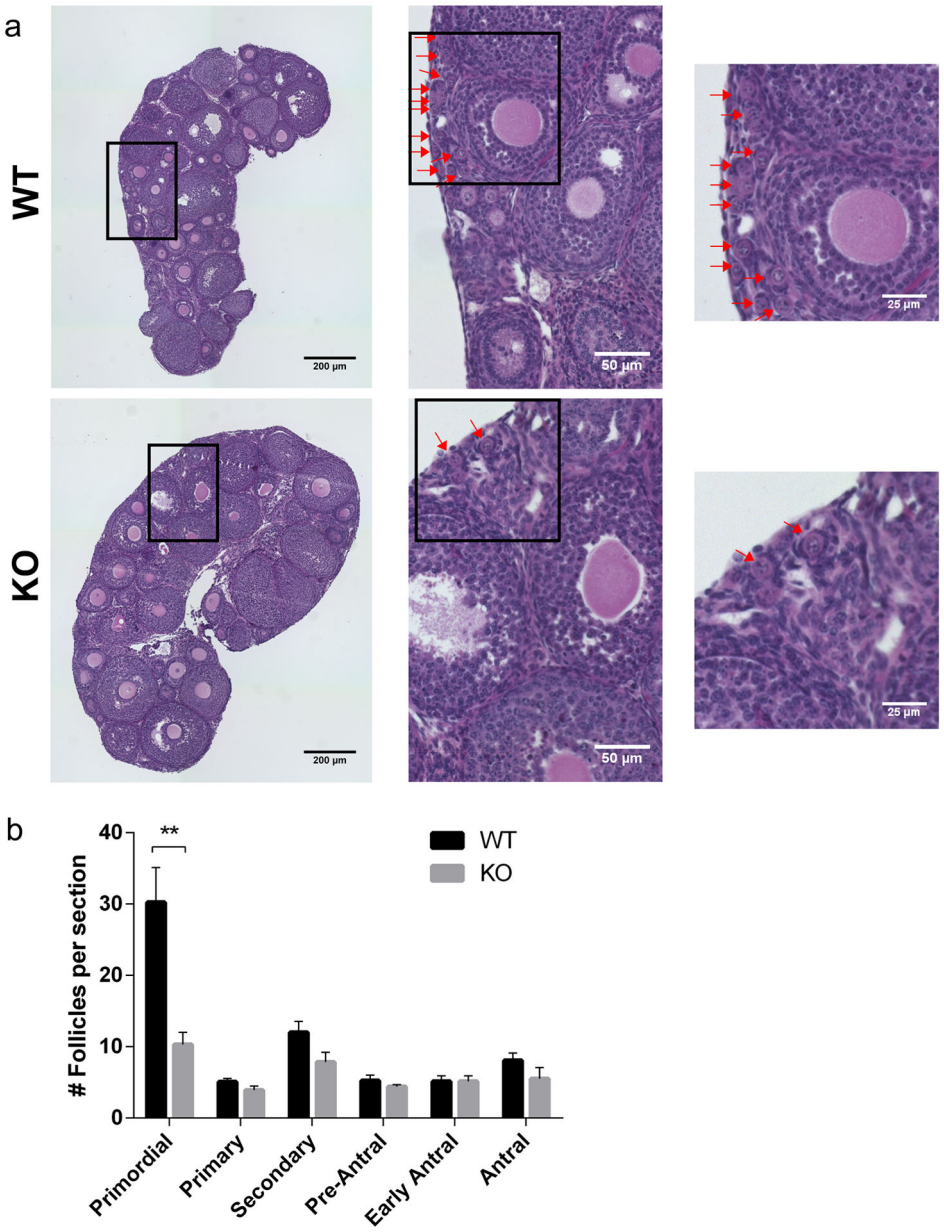

Fig. 3. Reduced number of primordial follicles in the absence of SIRT7

(a) Representative images of hematoxylin/eosin-stained ovarian sections from 3-week-old wild-type (WT) and *Sirt7*$^{-/-}$ (KO) females. Red arrows denote primordial follicles in all panels. The boxes indicate the regions of zoom. **(b)** Quantification of follicle types from the ovaries represented in (a). Follicle numbers were quantified for each ovary and reported as the average number of each type of follicles per section. Graph represents the mean ±SEM (n=4 animals/genotype). ** P < 0.01

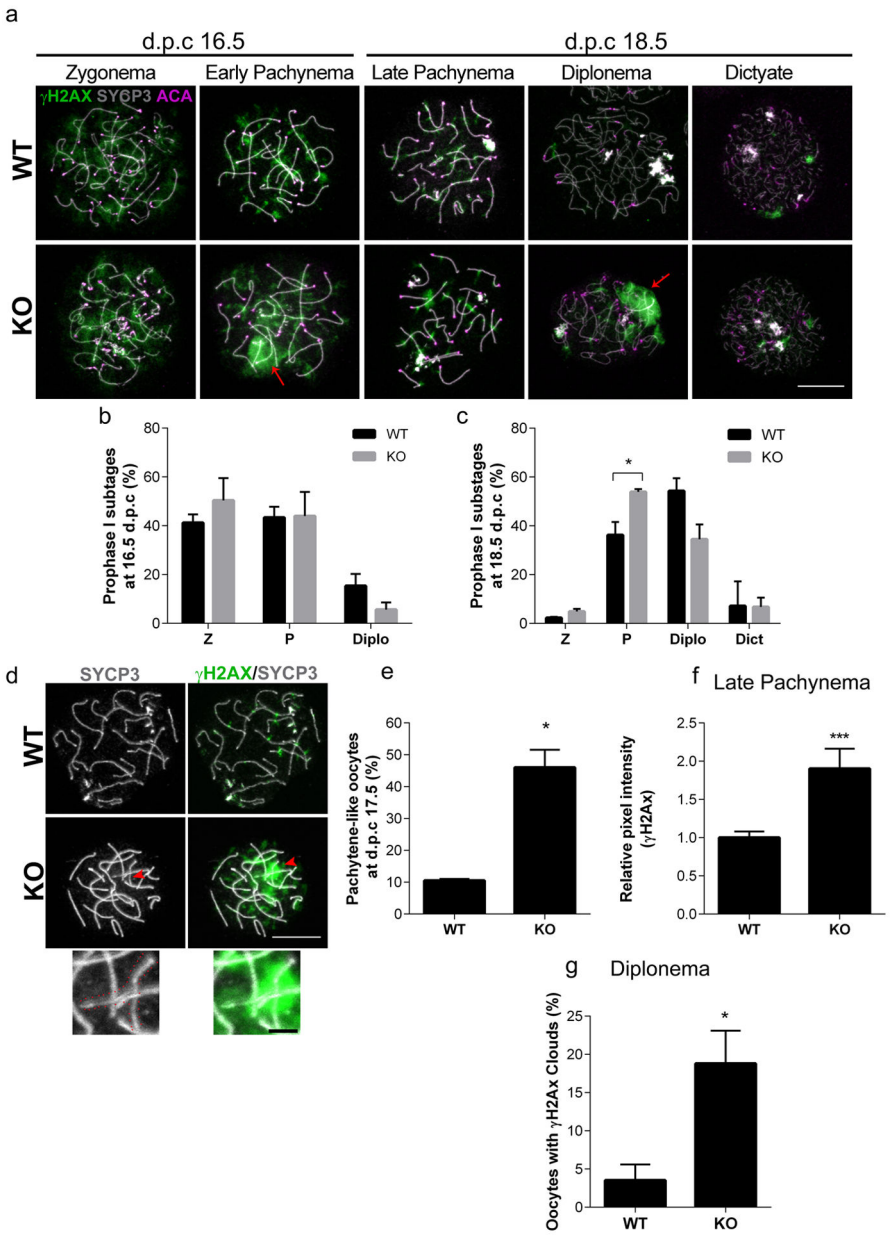

Fig. 4. *Sirt7*$^{-/-}$ oocytes have defects in γH2AX

(a) Representative images of prophase I substages in wild-type (WT) and *Sirt7*$^{-/-}$ (KO) ovaries at embryonic days (d.p.c., days *post coitum*) 16.5 and 18.5. γH2AX, green; SYCP3, gray; centromere (ACA), violet. Red arrows indicate clouds of γH2AX **(b-c)** Quantification of prophase I substages at embryonic days 16.5 (b) and 18.5 (c). Graph represents the mean ±SEM (n=3 experiments) Z, zygonema; P, pachynema; Diplo, diplonema; Dict, dictyate **(d)** Representative images of pachytene (WT) and pachytene-like (KO) oocytes at embryonic day 17.5. The red arrowhead points to the region of zoom. The red dotted lines outline the asynaptic chromosome in the zoom. **(e)** Percentage of pachynema-like oocytes WT and KO ovaries at embryonic day 17.5. (n=3 experiments, WT: 40, KO:58) **(f)** γH2AX average pixel intensity measured by the relative integrated density in late pachynema oocytes at embryonic

day 18.5. Graph represents the mean ±SEM (n=3 experiments, WT: 97, KO 105 oocytes) **(g)** Percentage of diplonema oocytes in WT and KO ovaries with clouds of γH2AX at embryonic day 18.5. Graph represents the mean ±SEM (n=3 experiments, WT: 80, KO 35 oocytes). *P<0.05; *** P < 0.001; scale bars, 10μm and 2μm in the zoom.

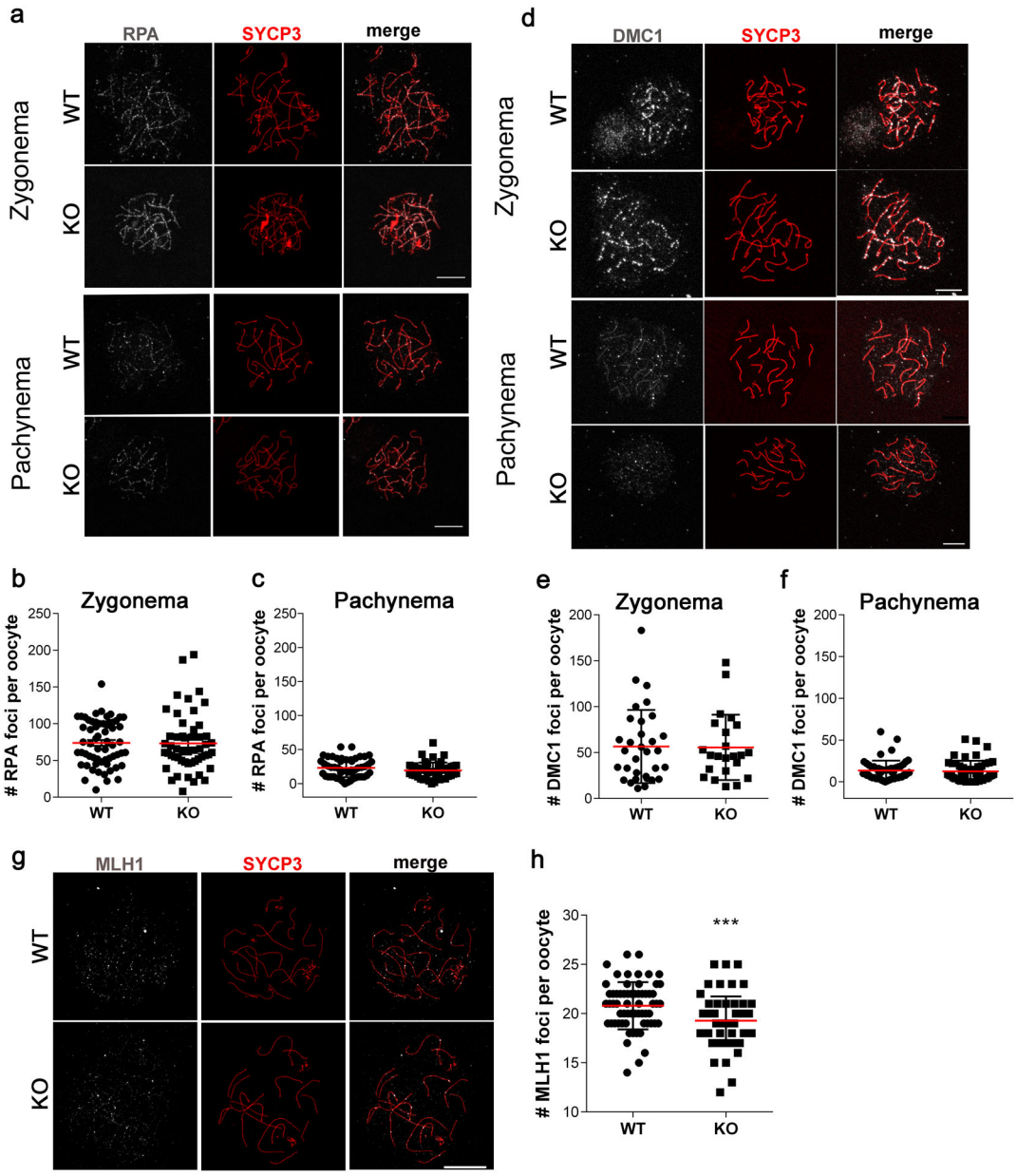

Fig. 5. Absence of *Sirt7* does not affect RPA or DMC1 foci formation but affects the number of cross over events

(a, d) Representative confocal images of zygotene and pachytene-staged oocytes immunostained with antibodies to detect SYCP3 (red) and RPA (gray) (a) or DMC1 (d) (gray) from wild-type (WT) and *Sirt7*$^{-/-}$ (KO) females at embryonic day 16.5. **(b-c)** Quantification of the number of RPA foci per oocyte at zygonema (b) (n=3 experiments, WT: 61, KO 52 oocytes) and pachynema (c) (n=3 experiments, WT: 51, KO 48 oocytes). **(e-f)** Quantification of the number of DMC1 foci per oocyte at zygonema (n=3 experiments, WT: 32, KO 23 oocytes) (e) and at pachynema (n=3 experiments, WT: 53, KO 51 oocytes) (f). **(g)** Representative confocal images of pachytene-staged oocytes immunostained with antibodies to detect SYCP3 (red) and MLH1 (gray) from WT and KO females at embryonic day 18.5. **(h)** Quantification of the number of MLH1 foci per oocyte at pachynema (n=3

experiments, WT: 63, KO 62 oocytes). Graph shows individuals values plus the mean ±SEM from 3 independent experiments. *** $P < 0.001$; scale bars, 10μm.

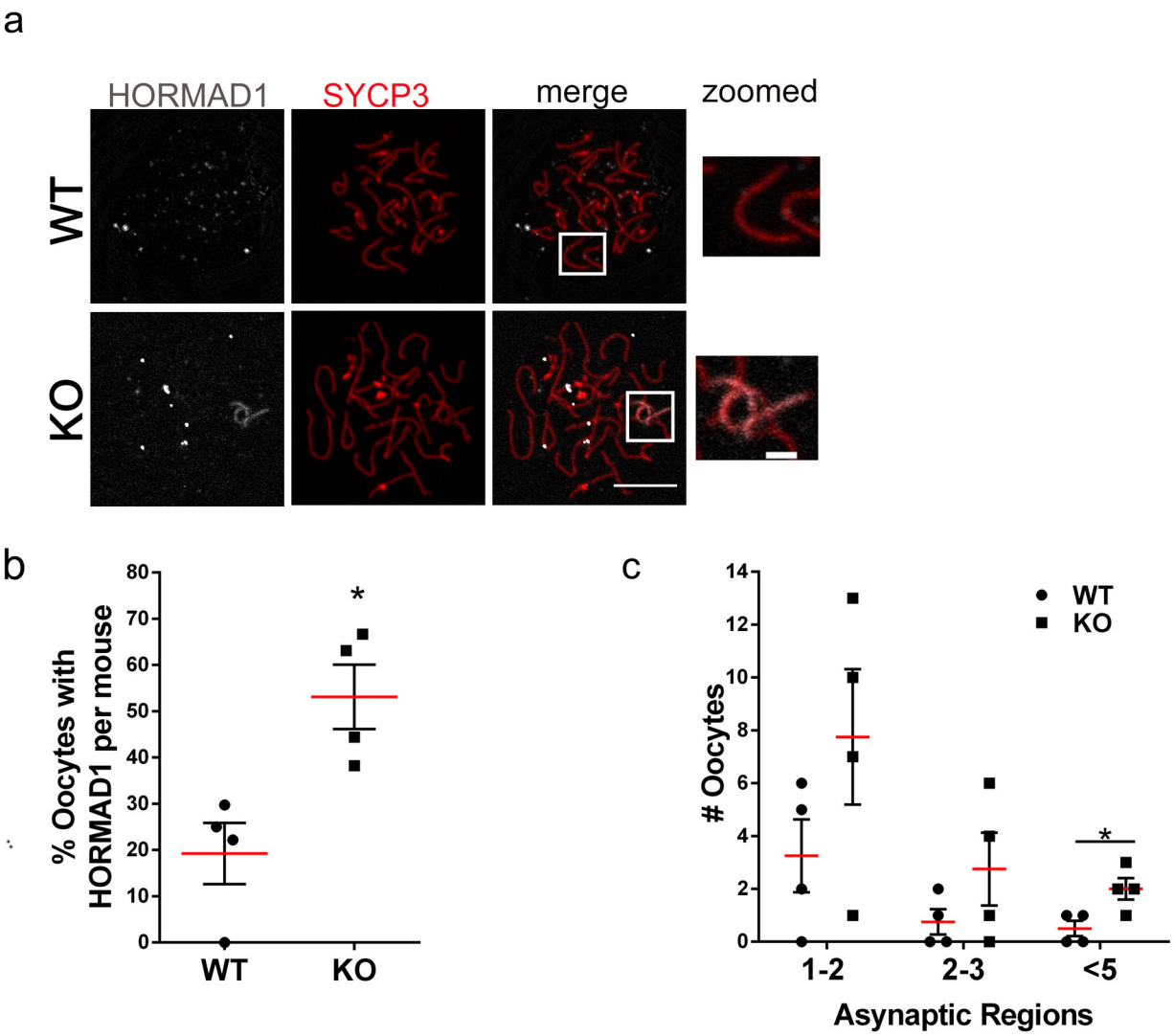

Fig. 6. SIRT7 deficient oocytes have impaired chromosome synapsis

(a) Representative confocal images of pachytene and pachytene-like-staged oocytes immunostained with antibodies to detect HORMAD1 (gray) and SYCP3 (red) from wild-type (WT) and *Sirt7*$^{-/-}$ (KO) females at embryonic day 17.5. The box indicates the region of zoom. **(b-c)** Percentage of pachytene oocytes with HORMAD1-positive staining (b) and number of cells with the indicated number of asynaptic regions (c). Graph represents the mean ±SEM from 4 independent experiments (~90 oocytes per genotype). * $P < 0.05$; scale bars, 10μm and 2μm in the zoom.

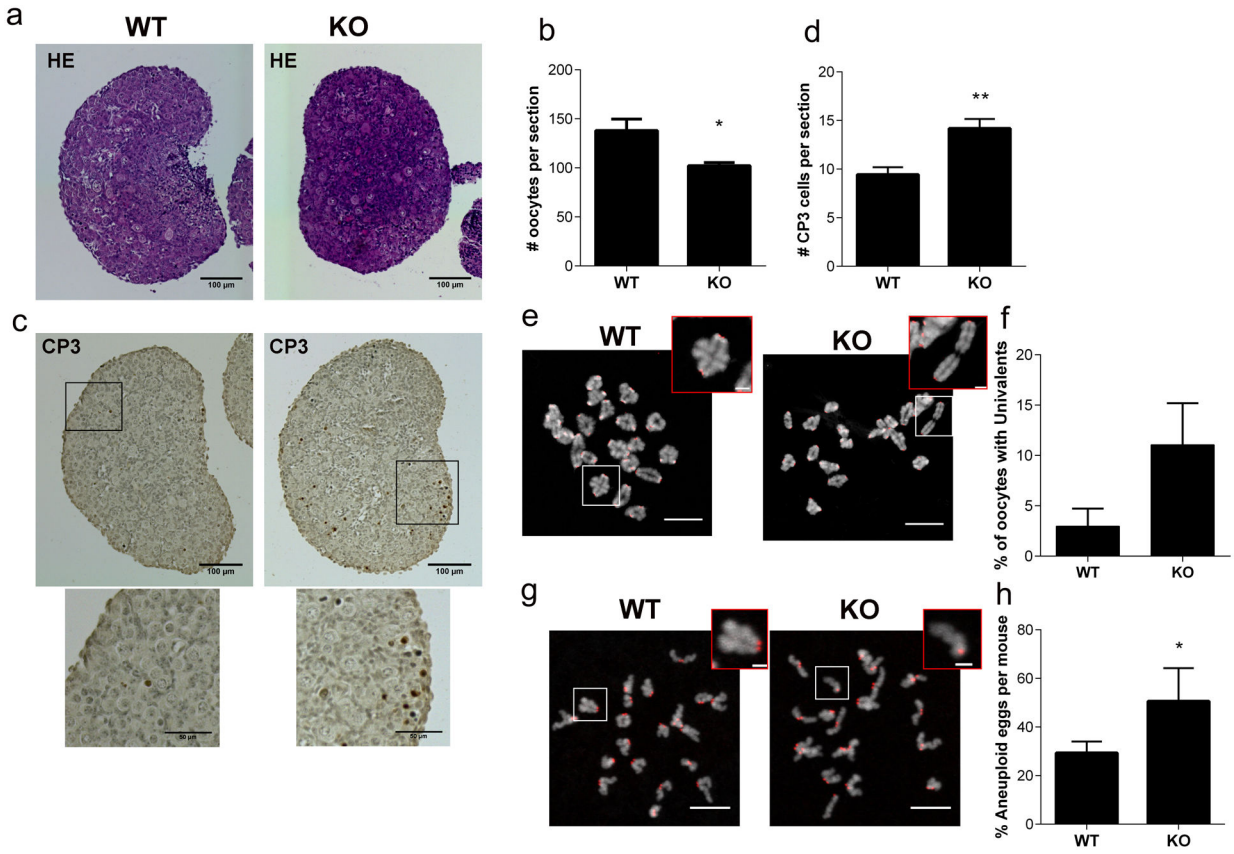

Fig. 7. Absence of *Sirt7* affects the ovarian reserve in neonates and increases aneuploidy levels in adults.

(a) Representative images of hematoxylin/eosin-stained (HE) ovarian sections from newborn wild-type (WT) and *Sirt7*$^{-/-}$ (KO) females. **(b)** Quantification of number of oocytes per section from the ovaries represented in (a) (n=4 animals/genotype). **(c)** Representative images of cleaved Caspase 3- (CP3), brown) stained ovarian sections from newborn WT and KOs. **(d)** Quantification of CP3 positive cells per section from the ovaries represented in (c) (n=4 animals/genotype). **(e)** Representative confocal images of metaphase I chromosome spreads. DNA, gray; centromeres (ACA), red. The white boxed regions indicate zoom. Zoomed insets show bivalent and univalent chromosomes in WT and KO, respectively. **(f)** Quantification of percentage of oocytes with univalents from (e) (n=4 animals/genotype WT:54, KO:36 oocytes). **(g)** Representative confocal images of *in situ* metaphase II chromosome spreads after monastrol treatment. DNA, gray; ACA, red. The white boxed regions indicate zoom. Zoomed insets show sister chromatids together and premature sister chromatid separation in WT and KO, respectively. **(h)** Percentage of aneuploid eggs per mouse in WT and KO females (WT: 4 animals, 76 eggs; KO: 3 animals 53 eggs). Graph represents the mean ±SEM. ** P < 0.01, * P < 0.05; scale bars, 10μm and 2μm for insets.

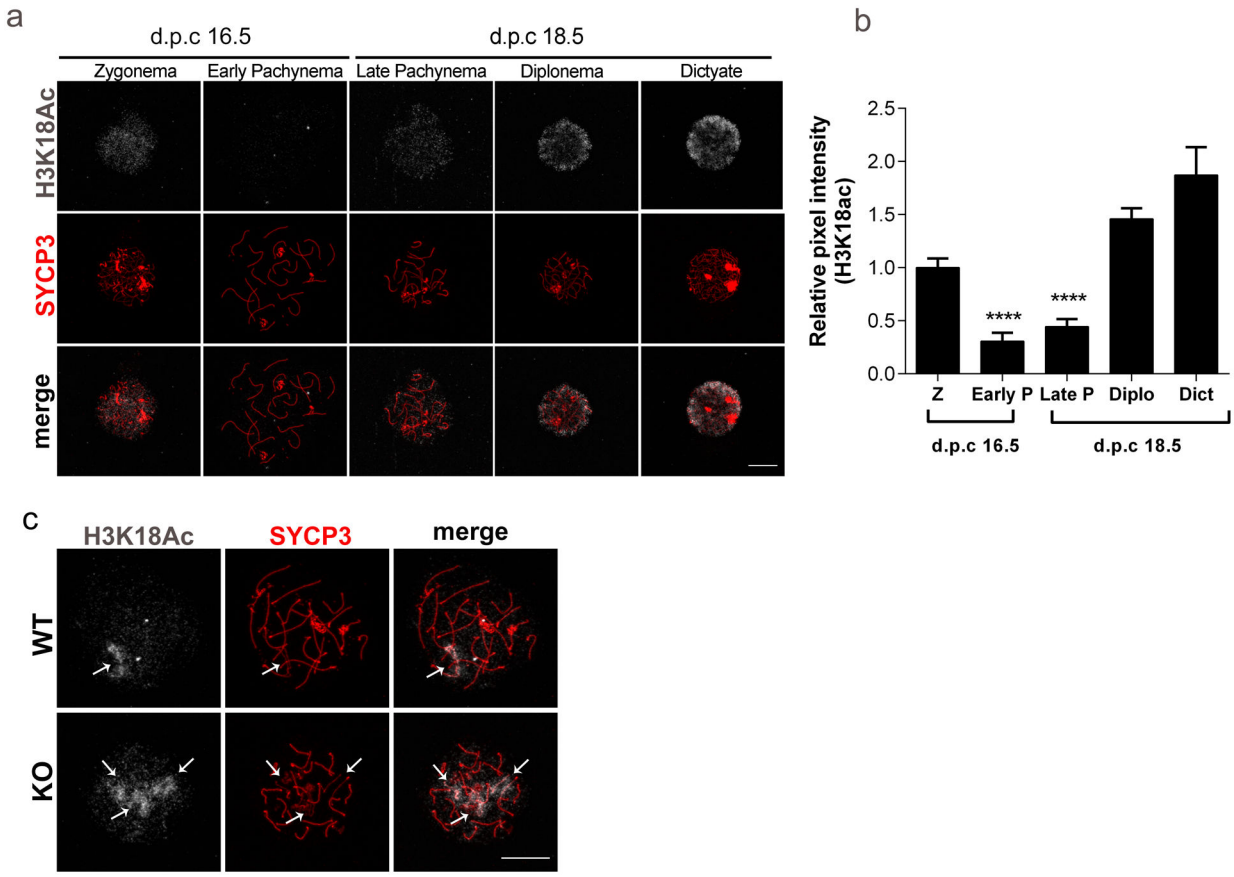

Fig. 8. Defects in deacetylation of H3K18 during pachytene correlates with regions of asynapsis

(a) Representative images of prophase I substages in wild-type (WT) ovaries at embryonic days (d.p.c., days *post coitum*) 16.5 and 18.5, stained with an antibody to detect acetylated lysine 18 of histone H3 (H3K18ac) (gray) and SYCP3 (red). **(b)** H3K18ac pixel intensity as measured by the relative integrated density from prophase I substages represented in (a). Z, zygotene; P, pachytene; Diplo, diplotene; Dict, dictyate. Graph represents the mean ±SEM (n=3 experiments). **(c)** Representative confocal images detecting H3K18ac (gray) and SYCP3 (red) in pachytene-like oocytes from WT and *Sirt7*$^{-/-}$(KO). ** P< 0.01; **** P< 0.0001. scale bar, 10μm